Pharmacological Research 187 (2023) 106634

Contents lists available at ScienceDirect

Pharmacological Research

journal homepage: www.elsevier.com/locate/yphrs

Mirabegron-induced brown fat activation does not exacerbate atherosclerosis in mice with a functional hepatic ApoE-LDLR pathway

Zhixiong Ying [a,b,1], Robin van Eenige [a,b,1], Rosa Beerepoot [a,b], Mariëtte R. Boon [a,b], Niels J. Kloosterhuis [c], Bart van de Sluis [c], Alexander Bartelt [d,e,f], Patrick C.N. Rensen [a,b], Sander Kooijman [a,b,*,2]

[a] Division of Endocrinology, Department of Medicine, Leiden University Medical Center, Leiden, the Netherlands
[b] Einthoven Laboratory for Experimental Vascular Medicine, Leiden University Medical Center, Leiden, the Netherlands
[c] Department of Pediatrics, University of Groningen, University Medical Center Groningen, Groningen, the Netherlands
[d] Institute for Cardiovascular Prevention (IPEK), Ludwig-Maximilians-University, Munich, Germany
[e] Institute for Diabetes and Cancer (IDC), Helmholtz Center Munich, Neuherberg, Germany
[f] German Center for Cardiovascular Research (DZHK), Partner Site Munich Heart Alliance, Technische Universität München, Munich, Germany

ARTICLE INFO

Keywords:
Atherosclerosis
Brown adipose tissue
Lipolysis
Lipoproteins
VLDL secretion
White adipose tissue

ABSTRACT

Activation of brown adipose tissue (BAT) with the β3-adrenergic receptor agonist CL316,243 protects mice from atherosclerosis development, and the presence of metabolically active BAT is associated with cardiometabolic health in humans. In contrast, exposure to cold or treatment with the clinically used β3-adrenergic receptor agonist mirabegron to activate BAT exacerbates atherosclerosis in apolipoprotein E (ApoE)- and low-density lipoprotein receptor (LDLR)-deficient mice, both lacking a functional ApoE-LDLR pathway crucial for lipoprotein remnant clearance. We, therefore, investigated the effects of mirabegron treatment on dyslipidemia and atherosclerosis development in APOE*3-Leiden.CETP mice, a humanized lipoprotein metabolism model with a functional ApoE-LDLR clearance pathway. Mirabegron activated BAT and induced white adipose tissue (WAT) browning, accompanied by selectively increased fat oxidation and attenuated fat mass gain. Mirabegron increased the uptake of fatty acids derived from triglyceride (TG)-rich lipoproteins by BAT and WAT, which was coupled to increased hepatic uptake of the generated cholesterol-enriched core remnants. Mirabegron also promoted hepatic very low-density lipoprotein (VLDL) production, likely due to an increased flux of fatty acids from WAT to the liver, and resulted in transient elevation in plasma TG levels followed by a substantial decrease in plasma TGs. These effects led to a trend toward lower plasma cholesterol levels and reduced atherosclerosis. We conclude that BAT activation by mirabegron leads to substantial metabolic benefits in APOE*3-Leiden.CETP mice, and mirabegron treatment is certainly not atherogenic. These data underscore the importance of the choice of experimental models when investigating the effect of BAT activation on lipoprotein metabolism and atherosclerosis.

Abbreviations: [^{14}C]CO, [^{14}C]cholesteryl oleate; [^{3}H]TO, glycerol tri[^{3}H]oleate; ACACA, acetyl-CoA carboxylase; APOB, apolipoprotein B; ADRB1, β1-adrenergic receptor; ADRB2, β2-adrenergic receptor; ADRB3, β3-adrenergic receptor; ANGPTL4, angiopoietin-like 4; APOE, apolipoprotein E; BAT, DPM, brown adipose tissuedisintegrations per minute; CD36, cluster of differentiation 36; CPT1A, carnitine palmitoyltransferase 1 α; DGAT1, diacylglycerol O-acyltransferase 1; DGAT2, diacylglycerol O-acyltransferase 2; E3L.CETP, APOE* 3-Leiden.CETP; CETP, cholesteryl ester transfer protein; FA, fatty acid; FASN, GAPDH, fatty acid synthase-glyceraldehyde 3-phosphate dehydrogenase; GPIHBP1, glycosylphosphatidylinositol anchored high density lipoprotein binding protein 1; HDL, high-density lipoprotein; HMGCR, 3-hydroxy-3-methylglutaryl-CoA reductase; iBAT, interscapular brown adipose tissue; LDL, low-density lipoprotein; LDLR, low-density lipoprotein receptor; LPL, lipoprotein lipase; MTTP, microsomal triglyceride transfer protein; PL, phospholipid; PPARA, peroxisome proliferator activated receptor α; sBAT, subscapular brown adipose tissue; SREBF2, sterol regulatory element-binding transcription factor 2; sWAT, subcutaneous white adipose tissue; TC, total cholesterol; TG, TRL, triglyceridetriglyceride-rich lipoprotein; UCP1, uncoupling protein 1; VLDL, very-low-density lipoprotein; β-AR, β-adrenergic receptor.

* Correspondence to: P.O. Box 9600, 2300 RC Leiden, the Netherlands.
E-mail address: s.kooijman@lumc.nl (S. Kooijman).
[1] Authors contributed equally.
[2] Visiting address: Albinusdreef 2, 2333ZA Leiden, the Netherlands

https://doi.org/10.1016/j.phrs.2022.106634
Received 22 September 2022; Received in revised form 9 December 2022; Accepted 23 December 2022
Available online 24 December 2022

1. Introduction

Atherosclerosis, the underlying pathology of many cardiovascular diseases, is characterized by the thickening, hardening, and loss of elasticity of the arterial wall. The main risk factor for atherosclerosis is dyslipidemia, which is defined as high plasma levels of low-density lipoprotein (LDL)-cholesterol, very-low-density lipoprotein (VLDL)-cholesterol and -triglycerides (TGs) with or without low high-density lipoprotein (HDL)-cholesterol levels [1]. As mice carry most of their cholesterol in HDLs with virtually absent TG-rich lipoprotein (TRL) remnant- and LDL-cholesterol, they do not naturally develop hypercholesterolemia and atherosclerosis, and thus genetic modifications are required to elicit and study these pathogenic processes. Mice genetically deficient in apolipoprotein E (ApoE) or LDL receptor (LDLR) display high plasma cholesterol levels and carry most of their cholesterol in TRL remnants or LDL [2], and are therefore often used as experimental models in atherosclerosis research.

Brown adipose tissue (BAT) is a highly active metabolic tissue that combusts TG-derived fatty acids (FAs) to produce heat. It is activated by cold, which stimulates sympathetic outflow toward the tissue [3]. At the level of the brown adipocyte, norepinephrine binds to and activates β-adrenergic receptors (β-ARs) on the adipocytic membrane, which induces rapid lipolysis of intracellular TGs. The released FAs are directed to mitochondria where they either undergo β-oxidation to generate a proton gradient across the inner mitochondrial membrane or allosterically activate uncoupling protein 1 (UCP1), which dissipates this proton gradient, resulting in the generation of heat instead of ATP. To replenish depleted lipid stores, thermogenic brown adipocytes take up a vast amount of FAs derived from extracellular lipolysis of TRLs [4]. For this reason, cold exposure and pharmacological entities such as β3-AR agonists have been shown to lower plasma TG concentrations in different mouse models [5,6]. Increased lipolytic processing of TRLs also accelerates the formation of cholesterol-enriched TRL remnants and LDL, and the extent to which the liver removes these pro-atherogenic lipoproteins is dominated by the acquisition of ApoE by the remnants to interact with the LDLR on hepatocytes. Due to the absence of this ApoE-LDLR pathway, BAT activation by cold exposure and by mirabegron, an FDA-approved β3-AR agonist to treat overactive bladder problems, increases plasma cholesterol levels and accelerates atherogenesis in both *Apoe*$^{-/-}$ and *Ldlr*$^{-/-}$ mice [7,8].

APOE*3-Leiden.CETP (E3L.CETP) mice express a naturally occurring variant of human APOE with attenuated LDLR binding on top of endogenous ApoE, as well as human cholesteryl ester transfer protein (CETP) that transfers cholesteryl esters from HDL to VLDL [9]. Therefore, E3L.CETP mice carry the majority of plasma cholesterol in TRL remnants while also having a functional hepatic ApoE-LDLR clearance pathway. As such, these mice are considered a model for human-like lipoprotein metabolism and atherosclerosis development, and respond to lipid-lowering strategies such as statin therapy [10] and PCSK9 inhibition [11]. Likewise, in this mouse model, BAT activation by the β3-AR agonist CL316,243 increases the formation as well as hepatic uptake of TRL remnants, thereby lowering non-HDL-cholesterol levels and reducing atherogenesis [6].

In the current study, we evaluated the effect of mirabegron on BAT activity in relation to lipoprotein metabolism and atherosclerosis in E3L.CETP mice. Apart from attenuating fat mass gain *via* increasing fat oxidation, mirabegron increased the uptake of TRL-TG-derived FAs by thermogenic adipocytes, which was coupled to accelerated hepatic clearance of TRL remnants. In addition, mirabegron increased hepatic VLDL-TG production. These combined effects result in nonsignificant reductions in hypercholesterolemia and atherosclerosis.

2. Materials and methods

2.1. Animals and treatment

All mouse experiments were performed in accordance with the Institute for Laboratory Animal Research Guide for the Care and Use of Laboratory Animals and had received approval from the National Committee for Animal Experimentation of the Netherlands ("Centrale Commissie Dierproeven"). Hemizygous APOE* 3-Leiden mice were crossbred with mice homozygously expressing human CETP to generate E3L.CETP mice (C57Bl/6 J background) as described before [9]. Ten to fourteen weeks old female E3L.CETP mice were housed under standard conditions with a 12 h:12 h light-dark cycle at 22 °C and *ad libitum* access to water and a Western-type diet containing 16% fat (15% cacao butter and 1% corn oil) and 0.1% cholesterol (ssniff Spezialdiäten GmbH). After a run-in period of 3 weeks, for each experiment, mice were divided into two experimental groups that were balanced for body weight, body composition, fasted plasma TG and total cholesterol (TC) levels and age using RandoMice v1.0.9 [12]. Mice received subcutaneous injections with mirabegron (8 mg·kg^{-1} body weight in around 100 μL; 223673–61–8, BOC Sciences) or vehicle (15% polyethylene glycol BioUltra 400 in PBS) corresponding to the high dose used by Sui et al. [8].

In experiment 1, mice (n = 16 per group) were injected with mirabegron or vehicle three times per week (Monday, Wednesday and Friday) for a total duration of 15 weeks. Body weight, body composition, as well as food intake (per cage) were monitored throughout the treatment. Tail vein blood was collected after 4 weeks (4-hour fasted), 8 weeks (unfasted), 12 weeks (4-hour fasted) and 15 weeks (4-hour fasted) of treatment. Mice were temporarily single-housed for indirect calorimetry during week 7 of treatment. After 15 weeks of treatment, 4-hour fasted mice received an intravenous injection with radiolabeled TRL-like particles to assess plasma clearance and organ uptake of lipids. Parts of the collected tissues were snap-frozen or formalin-fixed and paraffin-embedded. For part of the measurements/analyses, a predefined subset of n = 8 mice/samples per group was used.

In experiment 2, mice (n = 8 per group) were injected with mirabegron or vehicle five times per week (Monday-Friday). After 4 weeks of treatment, VLDL production was assessed in 4-hour fasted mice.

2.2. Body weight, body composition and food intake

Mice were weighed using a regular weighing scale and body composition was determined using an EchoMRI-100 (EchoMRI). Food intake was determined by weighing the food per cage and dividing the food consumption by the number of mice per cage.

2.3. Plasma lipid and glycerol levels

Plasma obtained after centrifugation was used to determine plasma TG (10166588130, Roche Diagnostics), TC (11489232216, Roche Diagnostics), free FAs (NEFA-HR(2), Fujifilm) and glycerol (2913, Instruchemie) using enzymatic kits. Apolipoprotein B (ApoB)-containing lipoproteins in plasma were precipitated by the addition of 20% polyethylene glycol 6000 in 200 mM glycine buffer (pH 10), and plasma HDL-cholesterol levels were determined by measuring TC in the supernatant. Non-HDL-cholesterol levels were calculated by subtracting HDL-cholesterol from TC.

2.4. Indirect calorimetry

Mice were individually housed in calorimetric home cages (Promethion Line; Sable Systems International). After 1 day of acclimatization, data on O_2 consumption rate and CO_2 production rate were collected every 5 min for 5 days in total. From these measurements, energy expenditure, fat oxidation and carbohydrate oxidation were calculated

as described before [6]. Physical activity was assessed through infrared beam breaks. At the end of the recording, body weight and composition were determined. Average values were calculated for the 24 h directly after administration of vehicle or mirabegron (Day of injection) and the 24 h thereafter (Day after injection).

2.5. In vivo plasma clearance and organ uptake of TRL-like particles

Glycerol tri[^{3}H]oleate ([^{3}H]triolein; [^{3}H]TO) and [^{14}C]cholesteryl oleate ([^{14}C]CO) double-labeled TRL-like particles were prepared as previously described [13] and injected into mice *via* their tail vein (1.0 mg TG per mouse in 200 μL PBS). Blood samples were drawn from the tail vein at 2, 5, 10, and 15 min after the particle injection. Subsequently, mice were killed by CO_2 inhalation, heart puncture blood was collected, and mice were perfused *via* the heart with ice-cold PBS to remove the blood and non-internalized particles from organs. (Parts of) organs and tissues (approx. 5–150 mg) were collected, weighed and dissolved overnight at 55 °C in 500 μL Solvable (Perkin Elmer). Plasma and dissolved organ/tissue samples were mixed with 2.5 mL and 5 mL Ultima Gold liquid scintillation cocktail (PerkinElmer), respectively, and ^{3}H and ^{14}C activity (disintegrations per minute, dpm) were quantified using a Tri-Carb 2910TR Low Activity Liquid Scintillation Analyzer (PerkinElmer). Plasma decay of [^{3}H]TO and [^{14}C]CO was expressed as the percentage of injected radioactive dose, where total plasma volume (mL) was estimated as 4.706% of body weight (g) [14]. Uptake of [^{3}H]TO- and [^{14}C]CO-derived radioactivity by organs was expressed as the percentage of injected radioactive dose per gram wet tissue.

2.6. Plasma insulin levels

In heart puncture plasma obtained after centrifugation, plasma insulin levels (Ultra Sensitive Mouse Insulin ELISA Kit, Crystal Chem) were determined using enzymatic kits.

2.7. BAT and WAT histology

Subscapular BAT (sBAT) and subcutaneous WAT (sWAT) were fixated in phosphate-buffered formaldehyde, embedded in paraffin and sectioned (5 μm). Tissue sections were incubated with an anti-UCP1 antibody (U6382; Sigma-Aldrich) and then an HRP-labeled secondary antibody (K4003; DAKO) that was captured and visualized by NovaRED™ HRP substrate (SK-4800; Vector Laboratories), and counterstained with Mayers Hematoxylin (1.09249; Merck). UCP1-positive areas and lipid areas (*i.e.*, unstained areas) were quantified using ImageJ software (version 1.52a) and expressed as the percentage of the lean area or total tissue area, respectively.

2.8. Gene expression analysis

Total RNA was extracted from snap-frozen liver samples (approx. 30–50 mg), interscapular BAT (iBAT) samples (approx. 10 mg) and sWAT samples (approx. 30 mg) using TriPure RNA Isolation Reagent (Roche). After measuring RNA concentration, 1 μg of RNA was reverse-transcribed into cDNA using Moloney Murine Leukemia Virus Reverse Transcriptase (M-MLV RT; Promega). Quantitative real-time PCR was performed using GoTaq® qPCR Master Mix (A6002; Promega) with a Bio-Rad CFX96 Touch™ Real-Time PCR Detection System. mRNA expression levels were normalized to *Gapdh* mRNA expression and expressed as fold change relative to the vehicle group using the $2^{-\Delta\Delta CT}$ method. Primer sequences are listed in Table 1.

2.9. Lipoprotein lipase activity assay

Snap-frozen iBAT and sWAT samples (approx. 10–20 mg) were manually cut with a razor blade and dissolved in DMEM (30 mg/mL; 31966, ThermoFisher Scientific) supplemented with 0.5% bovine serum albumin and 0.0004% heparin. After incubation (37 °C, 1 h), samples were centrifuged (16.2·g, 4 °C, 10 min) and the middle layer containing heparin-bound lipoprotein lipase (LPL) was used to assess LPL activity *in vitro*. Briefly, 200 μL substrate solution (9.2 mg/mL triolein (T7–140, Sigma), 6.7 μCi/mL [^{3}H]TO, 0.1% Triton X-100, 0.1 M Tris/HCl pH 8.6 (1.08382.100, Merck), 1% free FA-free bovine serum albumin (A6003, Sigma), and 20% heat-inactivated human serum) was added to 100 μL tissue extract. After 60 min, the reaction was stopped by addition of a mixture of heptane:methanol:chloroform (1:1.28:1.37 v·v^{-1}) and K_2CO_3 (0.1 M), after which ^{3}H-activity was measured as described before to calculate TG hydrolase activity.

Table 1
Primer sequences for quantitative real-time PCR.

Gene	Primers	
	Forward	Reverse
Acacα	AACGTGCAATCCGATTTGTT	GAGCAGTTCTGGGAGTTTCG
Angptl4	GGAAAGAGGCTTCCCAAGAT	TCCCAGGACTGGTTGAAGTC
ApoB	GCCCATTGTGGACAAGTTGATC	CCAGGACTTGGAGGTCTTGGA
Adrb1	TCGCTACCAGAGTTTGCT	GGCACGTAGAAGGAGACGAC
Adrb2	AACGACAGCGACTTCTTGCT	GCACACGCCAAGGAGATTAT
Adrb3	TGAAACAGCAGACAGGGACA	AGTCTGTCAGCTTCCCTCCA
Cd36	GCAAAGAACAGCAGCAAAATC	CAGTGAAGGCTCAAAGATGG
Cpt1α	GAGACTTCCAACGCATGACA	ATGGGTTGGGGTGATGTAGA
Dgat1	TCCGTCCAGGGTGGTAGTG	TGAACAAAGAATCTTGCAGACGA
Dgat2	TCGCGAGTACCTGATGTCTG	CTTCAGGGTGACTGCGTTCT
Fasn	GCGCTCCTCGCTTGTCGTCT	TAGAGCCCAGCCTTCCATCTCCTG
Gapdh	GGGGCTGGCATTGCTCTCAA	TTGCTCAGTGTCCTTGCTGGGG
Gpihbp1	CAGCAAACCCTTCTGCATCACG	AGTGTGGACTGGCAACAGGTCT
Hmgcr	CCGGCAACAACAAGATCTGTG	ATGTACAGGATGGCGATGCA
Lpl	CCCTAAGGACCCCTGAAGAC	GGCCCGATACAACCAGTCTA
Mttp	CTCTTGGCAGTGCTTTTTCTCT	GAGCTTGTATAGCCGCTCATT
Pparα	ATGCCAGTACTGCCGTTTTC	GGCCTTGACCTTGTTCATGT
Srebf2	TGAAGCTGGCCAATCAGAAAA	ACATCACTGTCCACCAGACTGC

2.10. Hepatic lipid content

Lipids were extracted from snap-frozen liver samples according to a modified protocol of Bligh and Dyer [15]. Briefly, liver samples (approx. 50 mg) were homogenized in CH_3OH (10 μL/mg tissue). To 45 μL homogenate, 1800 μL CH_3OH:$CHCl_3$ (1:3 v·v^{-1}) was added. The organic phase obtained after centrifugation (15 min; 20,000·g at room temperature) was dried with a gentle flow of gas N_2 and dissolved in 100 μL 2% Triton X-100 in $CHCl_3$. After the second drying step, obtained samples were dissolved in 100 μL H_2O for measurements. TG and TC were measured as described above, and phospholipids (PLs; 3009; Instruchemie) and protein (23225; Thermo Fisher Scientific) were measured using commercial kits. Hepatic lipids were expressed as nmol per mg protein.

Acacα, acetyl-CoA carboxylase α; *Angptl4*, angiopoietin-like 4; *ApoB*, apolipoprotein B; *Adrb1*, β1-adrenergic receptor; *Adrb2*, β2-adrenergic receptor; *Adrb3*, β3-adrenergic receptor; *Cd36*, cluster of differentiation 36; *Cpt1α*, carnitine palmitoyltransferase 1 α; *Dgat1*, diacylglycerol O-acyltransferase 1; *Dgat2*, diacylglycerol O-acyltransferase 2; *Fasn*, fatty acid synthase; *Gapdh*, glyceraldehyde 3-phosphate dehydrogenase; *Gpihbp1*, glycosylphosphatidylinositol anchored high density lipoprotein binding protein 1; *Hmgcr*, 3-hydroxy-3-methylglutaryl-CoA reductase; *Lpl*, lipoprotein lipase; *Mttp*, microsomal triglyceride transfer protein; *Pparα*, peroxisome proliferator activated receptor α; *Srebf2*, sterol regulatory element-binding transcription factor 2.

2.11. Atherosclerosis quantification

Collected hearts were fixed in phosphate-buffered formaldehyde, embedded in paraffin and cross-sectioned (5 μm) throughout the aortic root area. Per heart, four consecutive sections with 50 μm intervals were used for atherosclerosis measurements, starting from the appearance of

open aortic valve leaflets. Cross-sections were stained with hematoxylin-phloxine-saffron to determine lesion areas. Stained cross-sections were classified into diseased or undiseased sections and lesions were categorized into mild lesions (type I-III) and severe lesions (type IV-V) according to the guidelines of the American Heart Association adapted for mice [16]. Smooth muscle cells were stained using an anti-smooth muscle cell-actin antibody (M0851; Dako) and a second antibody EnVision+System-HRP Labelled Polymer (K4001; Dako) that was visualized by Liquid DAB+Substrate Chromogen System (K3468; Dako). Collagen was stained with 0.1% Direct Red 80 (365548; Sigma-Aldrich) and 0.1% Fast Green (F7258; Sigma-Aldrich) dissolved in saturated picric acid. Macrophage staining was performed with an anti-Mac-3 antibody (550292; BD Biosciences), an HRP-labeled secondary antibody (MP-7444, Vector Laboratories) and peroxidase substrate (SK-4800; Vector Laboratories). Lesion areas and the areas of smooth muscle cells, collagen and macrophages were determined using ImageJ software (version 1.52a).

2.12. Hepatic VLDL production rate

Mice were anesthetized *via* intraperitoneal injection with a mixture of 6.25 $mg{\cdot}kg^{-1}$ acepromazine, 6.25 $mg{\cdot}kg^{-1}$ midazolam and 0.31 $mg{\cdot}kg^{-1}$ fentanyl, followed by subcutaneous injection with 0.03 $mg{\cdot}kg^{-1}$ acepromazine, 0.03 $mg{\cdot}kg^{-1}$ midazolam and 0.001 $mg{\cdot}kg^{-1}$ fentanyl approximately every 45 min. Subsequently, mice were injected *via* the tail vein with 10 μCi Tran ^{35}S label (SCIS-103; Hartmann Analytic) to label newly synthesized ApoB and, 30 min later, with Triton WR 1339 (0.5 $g{\cdot}kg^{-1}$ body weight; T0307; Sigma-Aldrich) in PBS to prevent plasma TG hydrolysis. Fifteen minutes before and 15, 30, 60, and 90 min after Triton injection, blood was collected from the tail vein to measure plasma TGs as described above, and TG accumulation was plotted against time. Two hours after Triton injection, mice were exsanguinated *via* retro-orbital sinus to obtain serum, and VLDL was isolated after gradient ultracentrifugation at density= 1.006 $g{\cdot}mL^{-1}$. ^{35}S activity (dpm) was measured in VLDL and in the supernatant after precipitating VLDL-ApoB with 2-propanol by liquid scintillation counting (Ultima Gold, Perkin Elmer as liquid scintillation cocktail; Tri-Carb 2910 TR, PerkinElmer as scintillation counter) to calculate ^{35}S activity of VLDL-ApoB. VLDL-ApoB production was expressed as $dpm{\cdot}mL\ serum^{-1}{\cdot}hour^{-1}$. VLDL size was measured by dynamic light-scattering using a fixed-angle Zetasizer Nano ZSP (Malvern Instruments).

2.13. Isolation of primary hepatocytes

Primary hepatocytes were isolated from three chow-diet-fed female E3L.CETP mice according to a modified method of Wang et al. [17]. Briefly, the portal vein was cannulated and the liver was perfused at a flow rate of 6 $mL{\cdot}min^{-1}$ for approximately 1 h with a warm (37 °C) EDTA buffer containing 2.55 mM EDTA, 25 mM $NaHCO_3$, 16.48 mM glucose, 7.55 mM sodium L-lactate, 0.2 mM sodium pyruvate, 140 mM NaCl, 5 mM KCl, 0.8 mM $MgCl_2{\cdot}6\ H_2O$, 1.6 mM Na_2HPO_4 and 0.4 mM KH_2PO_4 and saturated with 95% O_2 and 5% CO_2. Cells were gently released and centrifuged (30 g, 21 °C, 4 min) to discard the supernatant. Hepatocytes were isolated from the remaining cell pellet after centrifugation (860 g, 21 °C, 6 min) in Percoll (P1644, Avantor) with average viability of approx. 95%. Pooled hepatocytes were cultured as previously described [18] with modifications as elaborated below.

2.14. Gene expression in primary hepatocytes

Primary hepatocytes were seeded into 12-well plates precoated with collagen at a density of 0.15×10^6 viable cells per well in 1 mL William's E medium (W4128; Sigma-Aldrich) supplemented with 10% fetal calf serum and 1% penicillin/streptomycin. Four hours later, nonattached cells were removed by careful washing with PBS. Cells were subsequently incubated with 1 mL William's E medium containing 1% penicillin/streptomycin and 0.75 mM oleate/0.5% BSA complex, and either remained untreated or were treated with 4 μM mirabegron, 4 μM formoterol or 4 μM isoprenaline for 4 h. After washing with PBS, hepatocytes were collected in 0.5 mL TriPure RNA Isolation Reagent (Roche) for gene expression measurement as described before. Primer sequences are listed in Table 1.

2.15. Lipid production in primary hepatocytes

Isolated hepatocytes were seeded into 6-well precoated plates at a density of 0.5×10^6 viable cells per well in 2 mL William's E medium supplemented with 10% fetal calf serum and 1% penicillin/streptomycin. Four hours later, nonattached cells were removed and the remaining cells were subsequently incubated with 2 mL William's E medium supplemented with 1% penicillin/streptomycin, containing 1 μCi/mL [^{3}H]oleate, 0.2 μCi/mL [^{14}C]acetic acid and 0.75 mM oleate/0.5% BSA complex, supplemented with or without 4 μM mirabegron, 4 μM formoterol or 4 μM isoprenaline. Therefore, lipids synthesized by hepatocytes from FAs and *via de novo* lipogenesis were labeled with ^3H and ^{14}C, respectively. After a 20-hour incubation, the medium was collected and hepatocytes were washed with PBS and then lysed and collected in 0.5 mL 0.1 M NaOH. Thereafter, 100 μL of each collected medium or cell sample was transferred into a 10 mL glass tube. Then, a mixture of 0.58 mL CH_3OH, 0.51 mL $CHCL_3$ and 0.41 mL heptane was added, followed by 0.5 mL 0.2 M NaOH. The mixture was vortexed until a miscible system was formed. Under the high pH environment generated by NaOH, hydrophobic free oleate (including [^{3}H]oleate) was transformed into hydrophilic Na-oleate. After centrifugation (1000 g, 21 °C, 10 min), the mixture was separated into two layers: a top aqueous layer containing hydrophilic components and a bottom organic layer containing hydrophobic lipids. After removing 0.9 mL of the aqueous layer, 0.5 mL 0.2 M NaOH was added to the glass tube again, and the vortexing and centrifugation were repeated so that more than 95% free [^{3}H]oleate and [^{14}C]acetic acid transmitted from the organic layer to the aqueous layer. ^3H and ^{14}C contents (dpm) were measured in 0.1 mL of the organic layer, which represented the amount of newly synthesized, [^{3}H]oleate- or [^{14}C]acetic acid-labeled lipids. Hepatocytes collected in 0.1 M NaOH were measured for protein content as mentioned above. Newly synthesized lipids in medium and hepatocytes were expressed as total [^{3}H]oleate- or [^{14}C]acetic acid-labeled lipids (dpm) per mg protein.

2.16. Statistical methods

Vehicle and mirabegron-treated groups were compared using unpaired two-tailed Student's t-tests. For the indirect calorimetry data, groups were compared using ANCOVA with body weight and body lean and fat mass as covariates. Simple linear regression was used to assess the relationship between uptake of ^{14}C activity in the liver and ^3H activity in BAT and to determine the VLDL-TG production rate. One-way ANOVA with Tukey post-hoc analysis was used to compare the effects of treatments on primary hepatocytes. Data are presented as mean ± SEM. *P* values less than 0.05 were considered statistically significant; *P* values less than 0.10 and greater than 0.05 were considered a trend.

3. Results

3.1. Mirabegron activates BAT and stimulates WAT browning, accompanied by more fat oxidation and attenuated fat mass gain

Dyslipidemic E3L.CETP mice were treated for 15 weeks with mirabegron or vehicle. Mirabegron activated BAT and induced WAT browning compared to vehicle, as evidenced by higher UCP1 protein content in sBAT (+30%; Fig. 1A-B) and sWAT (+190%; Fig. 1D-E). In addition, mice treated with mirabegron displayed less lipid content in both sBAT (Fig. 1 C) and sWAT (Fig. 1 F) than the control, indicative of enhanced lipid catabolism. Indeed, mirabegron increased energy

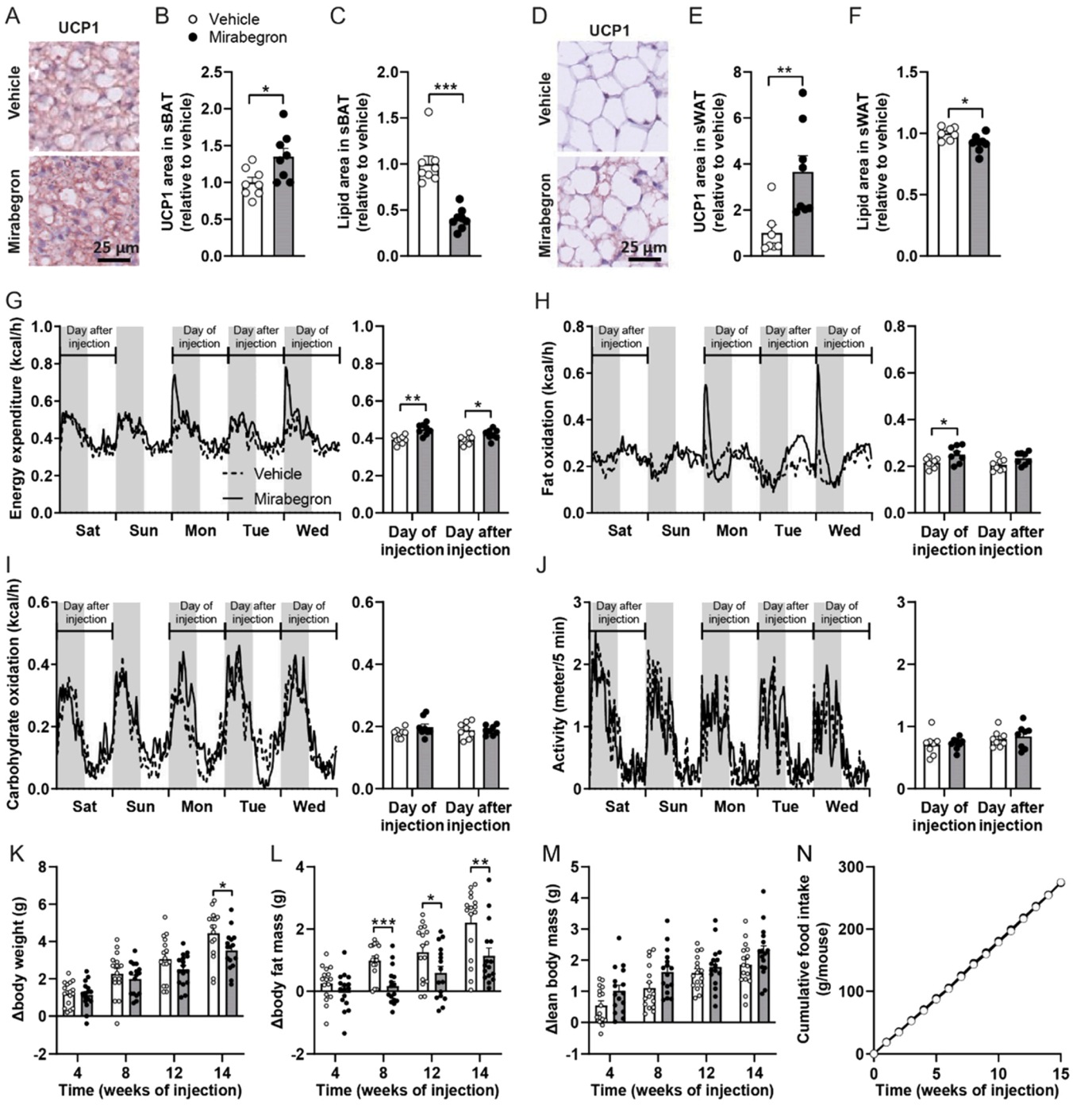

Fig. 1. Mirabegron activates brown adipose tissue and stimulates white adipose tissue browning, accompanied by increased fat oxidation and attenuated fat mass gain. Female APOE* 3-Leiden.CETP mice were fed a Western-type diet and injected with mirabegron or vehicle for 15 weeks. From a predefined subset of $n = 8$ mice per group, (A) subscapular brown adipose tissue (sBAT) and (D) subcutaneous white adipose tissue (sWAT) were stained for uncoupling protein 1 (UCP1), from which (B, E) UCP1 areas and (C, F) lipid areas were quantified. In week 7 of the injection, the mice were single-housed in calorimetric home cages in which O_2 consumption and CO_2 production were measured to determine (G) energy expenditure, (H) fat oxidation and (I) carbohydrate oxidation, and (J) physical activity was measured. (G-J) Averages per group are plotted over time; in addition, the averages of the 24 h following mirabegron or vehicle injections ("Day of injection") and the 24 h thereafter ("Day after injection") were summarized. Throughout the 15-week treatment, changes in (K) body weight, (L) body fat mass and (M) lean body mass as well as (N) cumulative food intake were monitored for all mice. Data are presented as mean ± SEM and individual data points, except for line graphs (A-C, $n = 8$ per group; D-F, $n = 7$–8 per group; K-M, $n = 16$ per group. N, derived from $n = 4$ cages per group). *$P < 0.05$, * *$P < 0.01$ and * **$P < 0.001$.

expenditure (day of injection: +14%; day after injection: +7%; Fig. 1 G) explained by a selective increase in fat oxidation reaching significance on the day of injection (+17%; Fig. 1H), while carbohydrate oxidation was unaltered compared to vehicle-treated mice (Fig. 1I). Mirabegron did not affect physical activity (Fig. 1 J). In line with the changes in energy expenditure, mirabegron attenuated body weight gain reaching statistical significance after 14 weeks of treatment (Fig. 1 K), which was explained by attenuation of body fat mass gain (Fig. 1 L) rather than lean body mass gain (Fig. 1 M). The prevention of fat mass gain was solely attributed to the increase in energy expenditure as mirabegron did not affect cumulative food intake (Fig. 1 N). Taken together, mirabegron activates thermogenic adipose tissues and stimulates energy expenditure

via selectively increasing fat oxidation, which attenuates fat mass gain.

3.2. Mirabegron lowers plasma triglycerides and tends to lower plasma cholesterol

Four-hour fasted plasma lipid levels were assessed after 4 and 12 weeks of treatment, approximately 20 h after the last injection with mirabegron or vehicle. Under these circumstances, mirabegron consistently decreased plasma TGs (Fig. 2 A). There was a trend for reduced plasma TC after 12 weeks of mirabegron treatment ($P = 0.065$; Fig. 2B) while plasma HDL-cholesterol was unaltered at either time point (Fig. 2 C). As a consequence, mirabegron tended to reduce non-HDL-cholesterol after 12 weeks of treatment ($P = 0.059$; Fig. 2D).

To study the acute effects of mirabegron, unfasted plasma was obtained 4 and 16 h after the last injection of week 8. Notably, mirabegron treatment showed time-dependent, opposite effects with a nonsignificant increase in plasma TGs 4 h after mirabegron injection (+40%, $P = 0.093$) followed by a pronounced decrease 16 h after the injection (−40%) (Fig. 2E). At either time point, mirabegron did not affect plasma TC levels (Fig. 2 F) and non-HDL-cholesterol levels (Fig. 2H), but elevated plasma HDL-cholesterol levels 16 h after the injection (Fig. 2 G). Overall, long-term treatment with mirabegron reduces TG and tends to reduce plasma TC and non-HDL-cholesterol.

3.3. Mirabegron stimulates lipolytic processing and hepatic clearance of TRLs

We next evaluated mirabegron-induced plasma clearance and organ uptake of TRL-TG-derived FAs and TRL remnants by injecting mice with TRL-mimicking particles doubled-labeled with [^{3}H]TO and [^{14}C]CO either 4 h (n = 8 mice per group) or 16 h (n = 8 mice per group) after the last injection of week 15. Mirabegron markedly accelerated plasma clearance of [^{3}H]TO (Fig. 3 A, E) explained by increased uptake of [^{3}H]TO-derived [^{3}H]oleate by BAT and WAT independent of time after the last injection (Fig. 3B, F). In sWAT collected 4 h after the last injection, no effect of mirabegron treatment was observed on the expression of *Lpl*, its anchoring protein glycosylphosphatidylinositol anchored high density lipoprotein binding protein 1 (*Gpihbp1*), the LPL-inhibitor angiopoietin-like 4 (*Angptl4*) or the FA-transporter cluster of differentiation 36 (*Cd36*), nor on LPL TG-hydrolase activity (Suppl. Fig. S1A-B). Interestingly, the expression of *Lpl*, *Gpihbp1* and *Angptl4* was lower in iBAT of mirabegron-treated mice. The net effect, however, was an increase in LPL TG-hydrolase activity (Suppl. Fig. S1C-D), which is in line with the strongly elevated uptake of [^{3}H]TO-derived [^{3}H]oleate by this tissue. The accelerated plasma clearance of [^{3}H]TO was accompanied by faster plasma clearance of [^{14}C]CO, representing TRL remnants, independent of the time after the last injection (Fig. 3 C, G). Interestingly, this seemed to be explained by higher retention of TRL remnants in BAT and WAT 4 h after the last injection (Fig. 3D), while increased uptake TRL of remnants by the liver was observed 16 h after the last injection with mirabegron (Fig. 3H). Regression analysis of combined data from both treatments and timepoints revealed that hepatic uptake of TRL remnants strongly correlated with the uptake of TRL-TG-derived FAs by BAT depots (Fig. 3I-K), indicating that increased lipolytic processing of TRLs by BAT is tightly coupled to TRL remnant clearance by the liver.

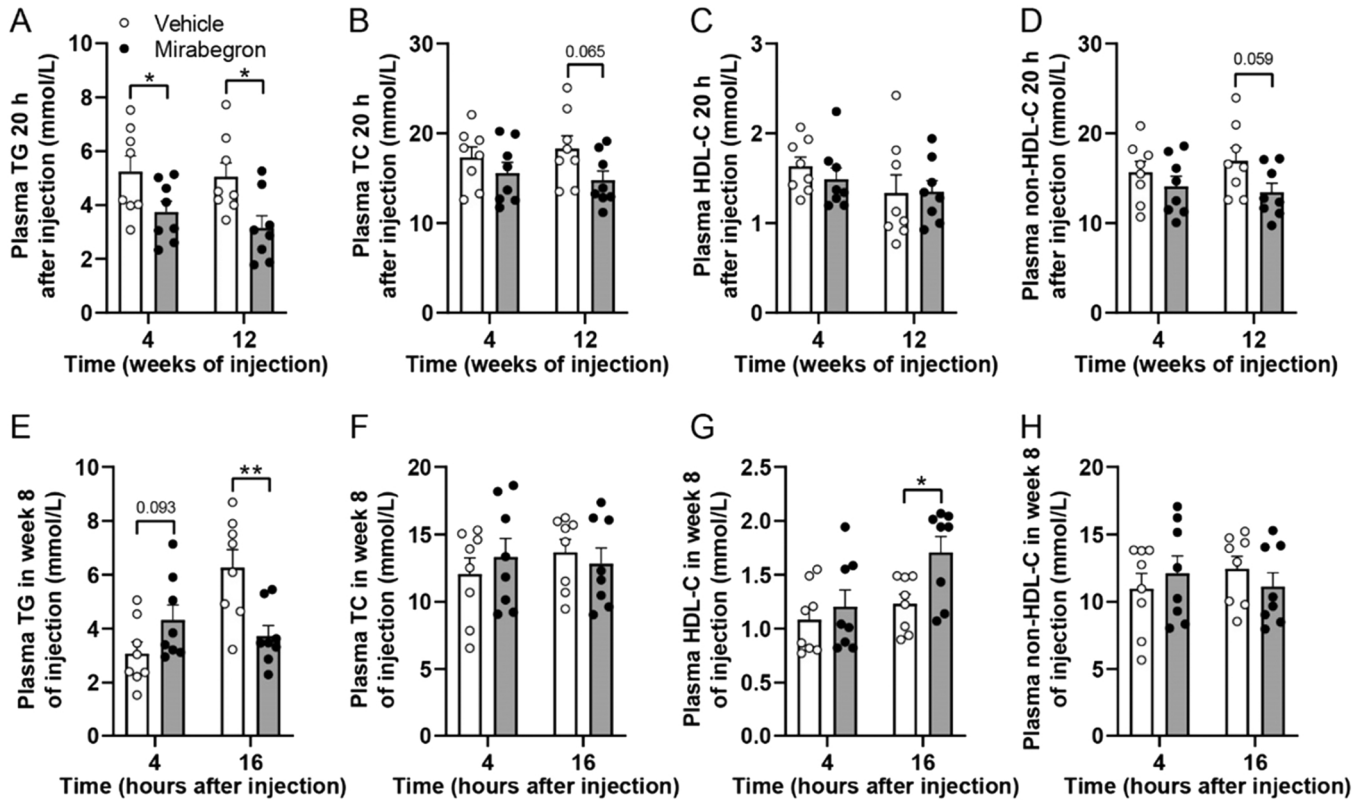

Fig. 2. Mirabegron lowers plasma triglycerides and tends to lower plasma cholesterol. Female APOE* 3-Leiden.CETP mice were fed a Western-type diet and injected with mirabegron or vehicle. In a predefined subset of $n = 8$ mice per group, after 4 and 12 weeks of the injection, 4 h-fasted plasma (A) triglycerides (TGs), (B) total cholesterol (TC) and (C) high-density lipoprotein-cholesterol (HDL-C) were determined, approximately 20 h after the last injection. (D) Non-HDL-C was calculated by subtracting HDL-C from TC. After 8 weeks of injection non-fasting plasma (E) TGs, (F) TC, (G) high-density lipoprotein-cholesterol (HDL-C) and (H) Non-HDL-C were determined/calculated 4 and 16 h after the last injection. Data are presented as mean ± SEM and individual data points ($n = 8$ per group). *$P < 0.05$ and * *$P < 0.01$.

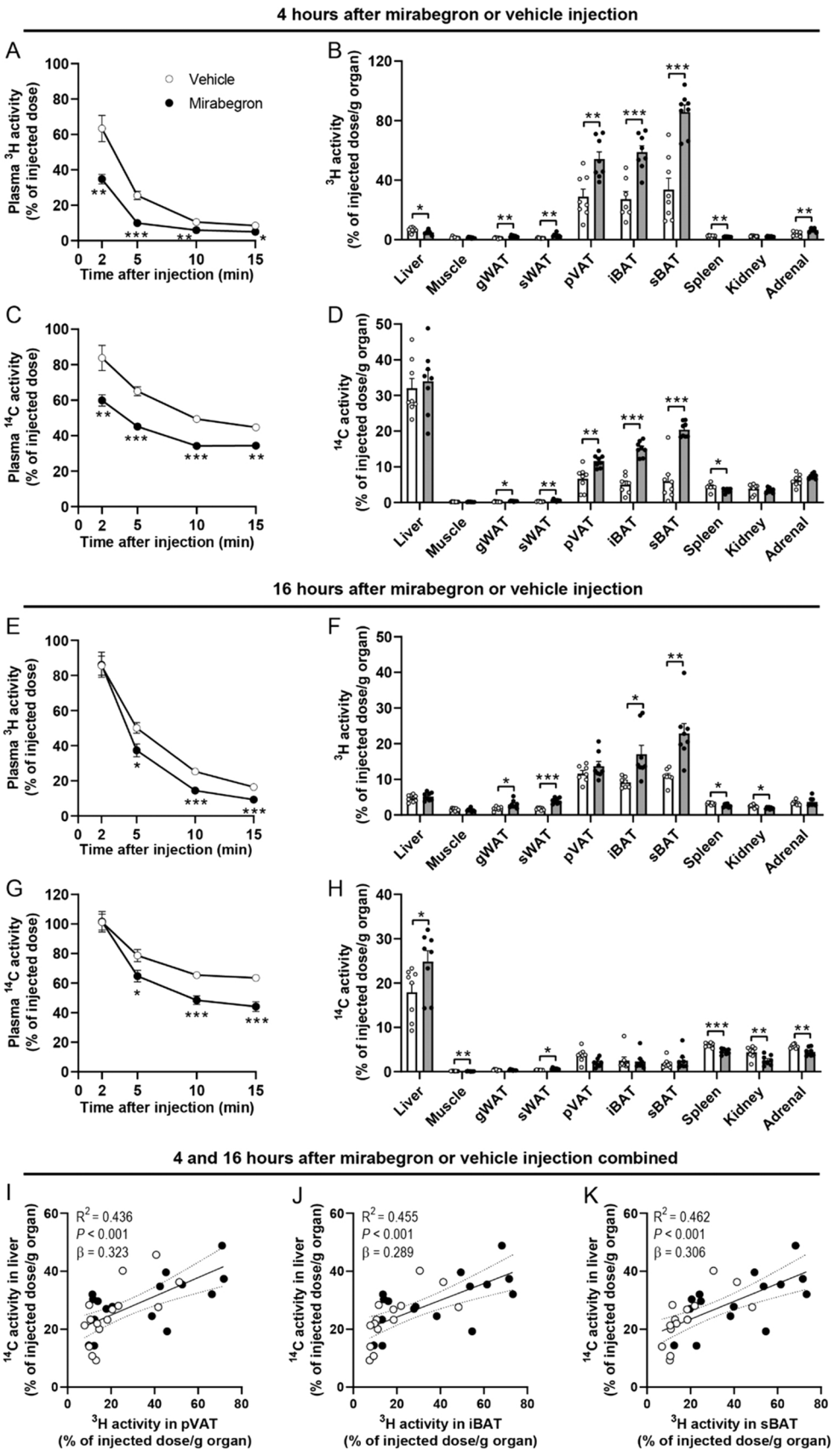

Fig. 3. Mirabegron stimulates lipolytic processing and hepatic clearance of triglyceride-rich lipoproteins. Female APOE* 3-Leiden. CETP mice were fed a Western-type diet and injected with mirabegron or vehicle for 15 weeks. In a predefined subset of $n = 8$ mice per group or in the remainder of $n = 8$ mice per group, respectively 4 or 16 h after the last injection, mice were fasted for 4 h followed by an injection with glycerol tri[^{3}H]oleate and [^{14}C]cholesteryl oleate double-labeled triglyceride-rich lipoproteins (TRL*s*)-mimicking particles to determine **(A, C, E, G)** the plasma decay and **(B, D, F, H)** organ uptake of TRL-TG-derived fatty acids (*i.e.*, [^{3}H] oleate) and the remnants (*i.e.*, [^{14}C]cholesteryl oleate). The hepatic uptake of [^{14}C] cholesteryl oleate was plotted against [^{3}H] oleate uptake by **(I)** perivascular adipose tissue (pVAT), **(J)** interscapular brown adipose tissue (iBAT) and **(K)** subscapular BAT (sBAT) and simple linear regression analyses were performed. Data are presented as mean ± SEM and individual data points (A, C, E and G, $n = 8$ per group; B, D and F, $n = 7$–8 per group; I-K $n = 30$–32 in total). *$P < 0.05$, * *$P < 0.01$ and * **$P < 0.001$.

3.4. Mirabegron increases hepatic VLDL production in vivo, but not in hepatocytes in vitro

Since mirabegron accelerated plasma TG clearance but tended to increase plasma TG levels 4 h after injection, we speculated that mirabegron may acutely increase VLDL-TG production. Analysis of livers collected 4 h after the last injection with mirabegron or vehicle at the end of the 15-week treatment period revealed that mirabegron largely increased the expression of genes involved in *de novo* lipogenesis (*i.e.*, *Acaca* and *Fasn*), but not the expression of genes involved in FA transport (*i.e.*, *Cd36*), TG synthesis (*i.e.*, *Dgat1* and *Dgat2*) or FA oxidation (*i.e.*, *Cpt1a* and *Pparα*) (Fig. 4 A). Additionally, mirabegron slightly upregulated the expression of *Mttp* involved in ApoB lipidation without affecting expression of *Apob* itself (Fig. 4 A). Mirabegron downregulated the expression of *Srebf2* and did not affect the expression of *Hmgcr*, both of which encode for proteins involved in cholesterol synthesis (Fig. 4 A). Strikingly, we observed that mirabegron caused a pronounced increase in plasma levels of free glycerol and free FAs (Fig. 4B), the majority of which is typically released by WAT [19,20] and taken up by the liver and used for hepatic TG synthesis and incorporation into VLDL [21]. Although FAs released upon intracellular lipolysis in WAT can stimulate insulin release by pancreatic β-cells [22], plasma insulin levels were not different between the groups 4 h after the last injection (Fig. 4 C). Despite an expected increased influx of glycerol and FAs toward the liver, mirabegron did not affect hepatic TG content and actually reduced TC (Fig. 4D). As measured after 4 weeks of treatment and 4 h after the last injection, mirabegron indeed increased hepatic VLDL-TG production (Fig. 4E), without affecting VLDL-ApoB production (Fig. 4 F), resulting in a larger average VLDL diameter (Fig. 4 G).

To exclude any direct effect of mirabegron on VLDL production, hepatocytes were isolated from chow diet-fed female E3L.CETP mice and cultured with or without mirabegron. Of the three β-AR subtypes, only mRNA expression of *Adrb2* encoding for the β2-AR could be detected (Fig. 4H). As cross-reactivity of mirabegron with the β2-AR has been reported [23], we continued by assessing the expression of genes involved in lipid synthesis and VLDL production. Mirabegron did not alter the expression of these genes, nor did the selective β2-AR agonist formoterol or the non-selective β-AR agonist isoprenaline (Fig. 4H). Interestingly, mirabegron treatment caused a nonsignificant reduction in [^{14}C]acetic acid-labeled lipids secreted into the culture medium (Fig. 4I-J), and significantly reduced the secretion of [^{3}H]oleate-labeled lipids in the medium (Fig. 4K-L). Formoterol and isoprenaline elicited comparable effects, suggesting that mirabegron exerts direct actions on the hepatocyte through β2-AR signaling. Nonetheless, it does not explain the strong increase in hepatic VLDL production observed upon mirabegron treatment *in vivo*, which is therefore most likely explained by the increased flux of FAs from WAT toward the liver.

3.5. Mirabegron tends to attenuate atherosclerosis development

Next, we determined atherosclerotic lesion size, as well as the lesion severity and composition in the root of the aortic arch after 15 weeks of treatment. Mirabegron tended to reduce atherosclerotic lesion size (−32%, $P = 0.097$; Fig. 5A-C) and did not change lesion severity (Fig. 5D). Mirabegron did not affect the number of diseased sections (Fig. 5E), lesion composition (*i.e.*, smooth muscle, collagen or macrophages areas within lesions; Fig. 5F-I) or lesion stability index (Fig. 5 J).

4. Discussion

Mirabegron is a clinically used β3-AR agonist which has been shown to activate BAT [8,24–28] and enhance energy expenditure [25,27–29] in mice and humans. A recent study reported that mirabegron exacerbated hypercholesterolemia and atherosclerosis in *Apoe*$^{-/-}$ and *Ldlr*$^{-/-}$ mice due to activation of thermogenic activity of BAT [8], based on which the authors raised concerns about the clinical use of mirabegron and BAT in general as a therapeutic target to protect against (cardio) metabolic diseases. Using E3L.CETP mice, a well-established model for human-like lipoprotein metabolism and atherosclerosis development with a functional ApoE and LDLR, we here demonstrate that mirabegron-induced BAT activation and WAT browning do not deteriorate, but rather tend to attenuate hypercholesterolemia and atherosclerosis development.

In this study, we first revealed that mirabegron activated BAT and promoted WAT browning in E3L.CETP mice, effects that were accompanied by selectively increased fat oxidation and reduced fat mass gain. In addition, we showed that treatment with mirabegron lowered plasma TG levels, an effect that is also observed in *Apoe*$^{-/-}$ and *Ldlr*$^{-/-}$ mice [8] and is explained by increased uptake of TRL-TG-derived FAs by BAT and WAT as demonstrated in the current study. In E3L.CETP mice, this increased TRL delipidation by the adipose tissues was coupled to enhanced hepatic uptake of TRL remnants as evident from the experiment performed 16 h after the last injection with mirabegron. These data are in line with previous studies in the same mouse model that also show accelerated hepatic remnant clearance upon stimulation of lipolytic activity in BAT following treatment with CL316,243 [6] or long-acting fibroblast growth factor 21 [30]. Here, we also observed high retention of TRLs remnants in BAT and WAT in the experiment performed 4 h after the last injection with mirabegron. This may be related to the high activation of BAT and WAT with prolonged retention of TLRs in the tissue fulfilling a high need for TG-derived FA uptake. The accelerated lipolytic processing of TRLs by BAT and WAT may furthermore increase the transfer of TRL-surface remnants to HDL, thereby improving HDL's cholesterol efflux-inducing capacity and subsequently increasing reverse cholesterol transport [31,32]. In line with this notion, we observed elevated HDL-cholesterol levels in mirabegron-treated mice.

Despite accelerated TG-derived FA uptake by thermogenic adipose tissues, plasma TG levels were not lowered 4 h after the injection with mirabegron. If any, TG levels were elevated at this time point, while they were markedly decreased 16 h after the injection. Additional experiments revealed that mirabegron induced an acute increase in hepatic VLDL-TG production, and a similar effect has been also reported before in *Apoe*$^{-/-}$ and *Ldlr*$^{-/-}$ mice [8]. In the current study, we additionally showed that the increase in VLDL-TG production was most likely not a direct effect of mirabegron on the liver as, if any, we observed a modest decrease rather than an increase in lipid synthesis and secretion in cultured primary hepatocytes upon mirabegron treatment, which was most likely explained by cross-activation of the β2-AR. Instead, we suggest the increase in VLDL-TG production to be the result of lipolysis in WAT upon mirabegron treatment and a subsequent increased FA flux toward the liver. In line with this notion, we did observe that treatment with mirabegron increased circulating levels of glycerol and free FAs while reducing WAT mass. Interestingly, a previous study has shown that FAs released upon WAT intracellular lipolysis after CL316,243 treatment acutely stimulate insulin release by pancreatic β-cells [22], which might explain the elevated hepatic expression of lipogenic genes. However, we found insulin levels to be unchanged 4 h after mirabegron treatment. As this may be a matter of timing, it would be of interest to investigate the even more acute effects of mirabegron on insulin levels.

Whilst the effects of mirabegron on TG metabolism were comparable between mouse models, the effects on cholesterol metabolism were very different between E3L.CETP mice and *Apoe*$^{-/-}$ and *Ldlr*$^{-/-}$ mice. In *Apoe*$^{-/-}$ and *Ldlr*$^{-/-}$ mice, TC and LDL-cholesterol are elevated upon mirabegron treatment [8], while in E3L.CETP mice we report a trend toward lower TC levels. This opposing effect is likely attributed to the fact that E3L.CETP mice have a functional ApoE-LDLR clearance pathway for TRL remnants, which is in favorable contrast to *Apoe*$^{-/-}$ and *Ldlr*$^{-/-}$ mice. In the absence of either ApoE or LDLR, BAT-stimulated TRL lipolysis causes the accumulation of cholesterol-enriched TRL remnants that causally accelerate atherosclerotic lesion development. Adding to this, in *Apoe*$^{-/-}$ and *Ldlr*$^{-/-}$ mice mirabegron has been reported to increase the hepatic *de*

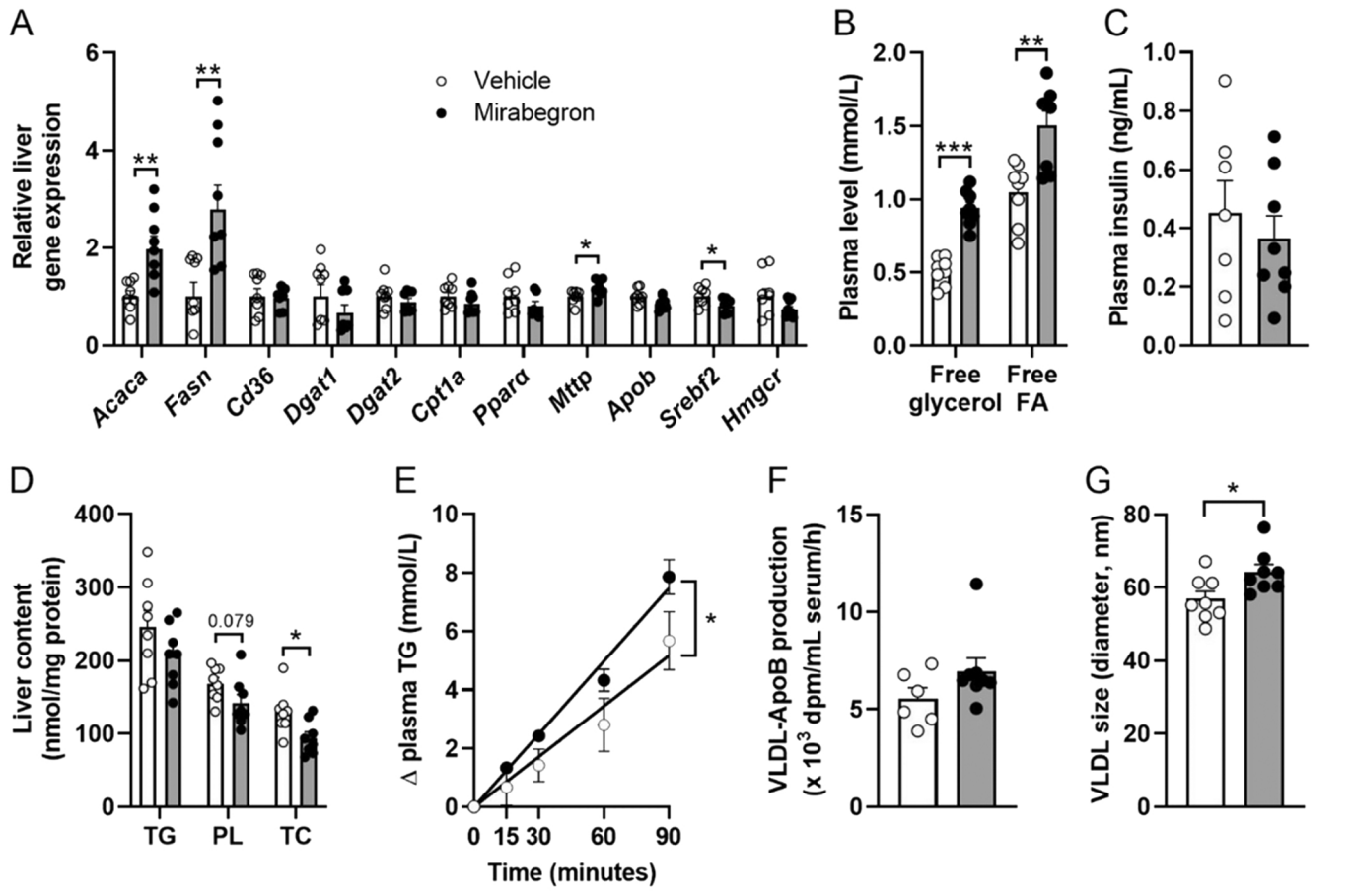

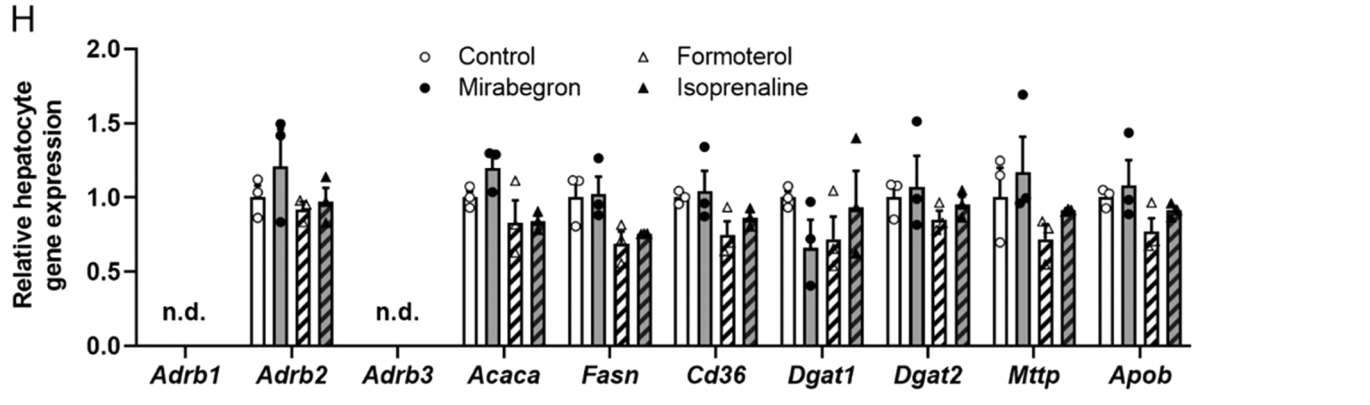

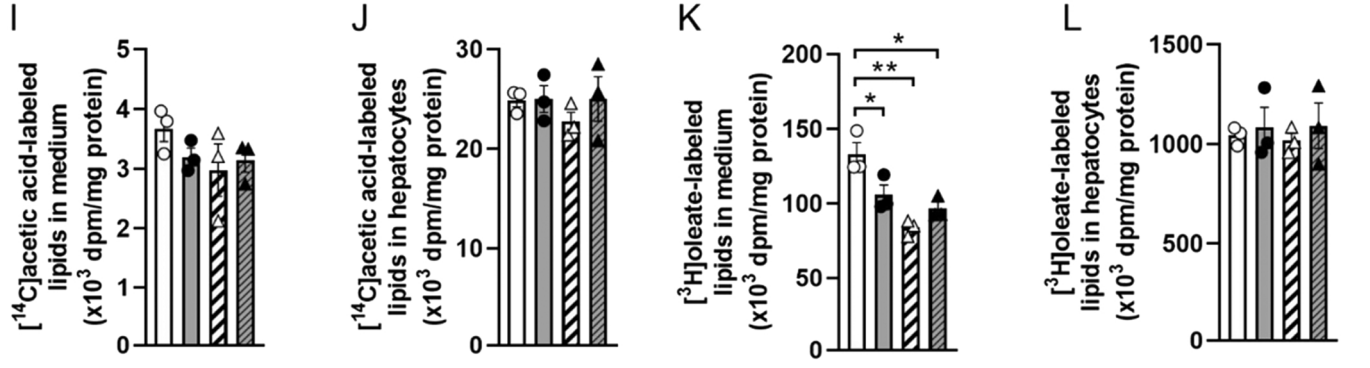

(caption on next page)

Fig. 4. Mirabegron increases hepatic very low-density lipoprotein production *in vivo*, but not in isolated hepatocytes *in vitro*. Female APOE* 3-Leiden.CETP mice were fed a Western-type diet and injected with mirabegron or vehicle for 15 weeks. In a predefined subset of $n = 8$ mice, (A) relative liver gene expression, (B) plasma levels of free glycerol, free fatty acids (FAs) and (C) insulin, as well as (D) the contents of liver triglycerides (TGs), phospholipids (PL) and total cholesterol (TC) were measured 4 h after the last injection and food deprivation. A separate cohort of female APOE* 3-Leiden.CETP mice were fed the same diet and injected with mirabegron or vehicle for 4 weeks. Four hours after the last treatment, *in vivo* hepatic very low-density lipoprotein (VLDL) production was determined by injection of Tran[^{35}S] label followed by Triton WR1339. (E) Plasma TG level changes from baseline, (F) VLDL-apolipoprotein B (ApoB) production and (G) VLDL size were assessed. Hepatocytes were isolated from chow diet-fed female APOE* 3-Leiden.CETP mice, cultured and treated with or without mirabegron, formoterol or isoprenaline. (H) After 4 h of treatment, hepatocytes were collected and relative gene expression were measured. In another batch of cultured hepatocytes treated with or without mirabegron, formoterol or isoprenaline, [^{3}H]oleate and [^{14}C]acetic acid were used to label newly synthesized lipids, to measure the accumulation of (I-J) [^{14}C]acetic acid- and (K-L) [^{3}H]oleate-labelled lipids in culture medium or hepatocytes. Data are presented as mean ± SEM and individual data points (A-B, D-E and G, $n = 8$ per group; C, F, $n = 6$ or 8 per group; H-L, $n = 3$ per group).*$P < 0.05$, * *$P < 0.01$. *Acaca*, Acetyl-CoA carboxylase 1; *Adrb1*, β1-adrenergic receptor; *Adrb2*, β2-adrenergic receptor; *Adrb3*, β3-adrenergic receptor; *Apob*, apolipoprotein B; *Cd36*, cluster of differentiation 36; *Cpt1a*, carnitine palmitoyltransferase 1a; *Dgat1*, diacylglycerol O-Acyltransferase 1; *Dgat2*, diacylglycerol O-Acyltransferase 2; *Fasn*, fatty acid synthase; *Hmgcr*, 3-hydroxy-3-methylglutaryl-CoA reductase; *Mttp*, microsomal triglyceride transfer protein; *Pparα*, peroxisome proliferator-activated receptor α; *Srebf2*, sterol regulatory element-binding transcription factor 2; n. d. not detectable (*i.e.*, CT value > 33).

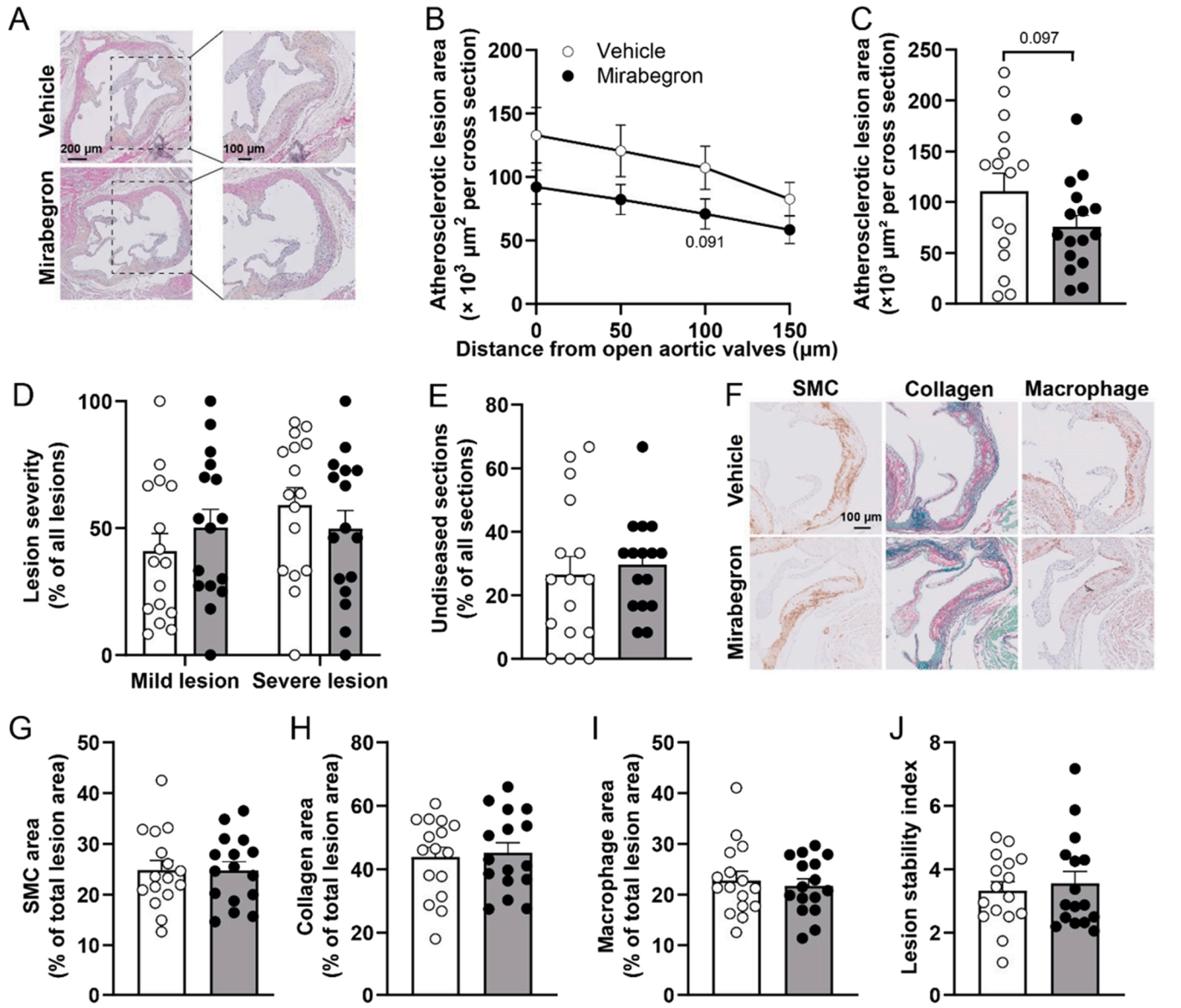

Fig. 5. Mirabegron tends to attenuate atherosclerosis development. Female APOE* 3-Leiden.CETP mice were fed a Western-type diet and injected with mirabegron or vehicle for 15 weeks. At the end of the treatment period, (A) the valve area of the aortic root was stained with hematoxylin-phloxine-saffron to vasualize atherosclerotic lesions. (B) The lesion areas were plotted as a function of distance from the appearance of open aortic valve leaflets covering 150 μm, from which (C) the mean atherosclerotic lesion areas were calculated. (D) Atherosclerotic lesions were categorized according to lesion severity and expressed as a percentage of total lesions, and (E) the percentage of undiseased sections was determined. The valve area of the aortic root were also stained for (F) smooth muscle cell (SMC), collagen and macrophages, and (G-I) their percentage areas relative to total lesion areas were calculated. In addition, (J) the stability index (the sum of collagen and smooth muscle cell areas as a fraction of macrophage areas) was calculated. Data are presented as mean ± SEM and individual data points ($n = 16$ per group).

novo cholesterol synthesis and to increase food intake (*i.e.*, reflecting increased cholesterol intake) [8]. These effects are likely triggered to compensate for the resulting decrease in hepatic cholesterol levels due to the defective hepatic uptake of TRL remnants. Indeed, in E3L.CETP mice we found no evidence for increased hepatic cholesterol synthesis or food intake upon mirabegron treatment.

Finally, we observed that mirabegron tended to reduce atherosclerosis development. This is in contrast with the large increase in atherosclerosis observed in *Apoe*$^{-/-}$ and *Ldlr*$^{-/-}$ mice [8]. Such reported proatherogenic effects probably do not reflect physiology of the general human population, since humans have an ApoE-LDLR pathway for TRL remnant clearance that is only disturbed in a minor fraction of the population due to genetic loss of function of ApoE (*i.e.*, familial dysbetalipoproteinemia) or LDLR (*i.e.*, familial hypercholesterolemia). Given that E3L.CETP mice closely reflect human physiology with respect to ApoE-mediated TRL remnant clearance by the hepatocytic LDLR, the non-significant reduction in atherosclerosis likely predicts the potential effects of BAT activation on atherosclerotic cardiovascular disease in humans. Indeed, previous studies have demonstrated that the presence of (cold-activated) BAT is associated with a lower prevalence of cardiovascular events [33,34] and better cardiovascular health in humans [33,35]. A recent study revealed that BAT in humans is activated by the β2-AR rather than the β3-AR as in mice [23]. This finding explains why β3-AR agonists to activate BAT lack efficacy in increasing energy expenditure in humans [36,37] and why 200 mg of mirabegron that leads to cross-activation of β2-AR activates human BAT while the 50 mg dose that activates β3-AR in the bladder does not have effect [23]. We foresee that pharmacological strategies, *e.g.* those targeting the β2-AR, may provide effective therapeutic handles to activate human BAT and thereby lower atherosclerotic cardiovascular disease risk in individuals with a functional ApoE-LDLR clearance pathway.

In conclusion, apart from attenuating body fat mass gain *via* increasing fat oxidation, mirabegron accelerates TRL turnover in BAT and WAT, resulting in an improved lipoprotein profile associated with a non-significant reduction of atherosclerotic lesion size in E3L.CETP mice with a functional ApoE-LDLR pathway for hepatic uptake of TRL remnants. Detrimental effects observed with mirabegron in *Apoe*$^{-/-}$ and *Lldr*$^{-/-}$ mice are thus likely attributed to the absence of hepatic TRL remnant clearance in those experimental models.

Funding

This work was supported by the Dutch Heart Foundation (2017T016 to S.K.) and the Netherlands Cardiovascular Research Initiative: an initiative with support of the Dutch Heart Foundation (CVON-GENIUS-2 to P.C.N.R. and B.V.D.S.). Z.Y. is supported by a full-time PhD scholarship from the China Scholarship Council (201806850094 to Z.Y.). A.B. is supported by the DFG CRC1123 project B10.

Author contributions

Conceptualization: Z.Y., R.V.E., P.C.N.R. and S.K.; Data curation: Z.Y., R.V.E. and R.B.; Formal analysis: Z.Y., R.V.E. and R.B.; Investigation: Z.Y., R.V.E., R.B, M.R.B, N.J.K., B.V.D.S., A.B. and S.K.; Writing – original draft: Z.Y; Writing – review & editing: Z.Y., R.V.E., P.C.N.R. and S.K.; Supervision, S.K.; Funding acquisition, P.C.N.R and S.K. Both Z.Y. and R.V.E. contributed equally and have the right to list their name first in their CV.

Declarations of interest

none.

Data Availability

Data will be made available on request.

Acknowledgements

The graphical abstract was created with BioRender.com.

Appendix A. Supporting information

Supplementary data associated with this article can be found in the online version at doi:10.1016/j.phrs.2022.106634.

References

[1] National Cholesterol Education Program (NCEP) Expert Panel on Detection, Evaluation, and Treatment of High Blood Cholesterol in Adults (Adult Treatment Panel III) Third Report of the National Cholesterol Education Program (NCEP) Expert Panel on Detection, Evaluation, and Treatment of High Blood Cholesterol in Adults (Adult Treatment Panel III) final report, Circulation 106 (25) (2002) 3143–3421.
[2] G.S. Getz, C.A. Reardon, Do the Apoe-/- and Ldlr-/- Mice Yield the Same Insight on Atherogenesis? Arterioscler. Thromb. Vasc. Biol. 36 (9) (2016) 1734–1741.
[3] B. Cannon, J. Nedergaard, Brown adipose tissue: function and physiological significance, Physiol. Rev. 84 (1) (2004) 277–359.
[4] P.P. Khedoe, G. Hoeke, S. Kooijman, W. Dijk, J.T. Buijs, S. Kersten, L.M. Havekes, P.S. Hiemstra, J.F. Berbee, M.R. Boon, P.C. Rensen, Brown adipose tissue takes up plasma triglycerides mostly after lipolysis, J. Lipid Res 56 (1) (2015) 51–59.
[5] A. Bartelt, O.T. Bruns, R. Reimer, H. Hohenberg, H. Ittrich, K. Peldschus, M. G. Kaul, U.I. Tromsdorf, H. Weller, C. Waurisch, A. Eychmuller, P.L. Gordts, F. Rinninger, K. Bruegelmann, B. Freund, P. Nielsen, M. Merkel, J. Heeren, Brown adipose tissue activity controls triglyceride clearance, Nat. Med 17 (2) (2011) 200–205.
[6] J.F. Berbee, M.R. Boon, P.P. Khedoe, A. Bartelt, C. Schlein, A. Worthmann, S. Kooijman, G. Hoeke, I.M. Mol, C. John, C. Jung, N. Vazirpanah, L.P. Brouwers, P. L. Gordts, J.D. Esko, P.S. Hiemstra, L.M. Havekes, L. Scheja, J. Heeren, P.C. Rensen, Brown fat activation reduces hypercholesterolaemia and protects from atherosclerosis development, Nat. Commun. 6 (2015) 6356.
[7] M. Dong, X. Yang, S. Lim, Z. Cao, J. Honek, H. Lu, C. Zhang, T. Seki, K. Hosaka, E. Wahlberg, Cold exposure promotes atherosclerotic plaque growth and instability via UCP1-dependent lipolysis, Cell Metab. 18 (1) (2013) 118–129.
[8] W. Sui, H. Li, Y. Yang, X. Jing, F. Xue, J. Cheng, M. Dong, M. Zhang, H. Pan, Y. Chen, Y. Zhang, Q. Zhou, W. Shi, X. Wang, H. Zhang, C. Zhang, Y. Zhang, Y. Cao, Bladder drug mirabegron exacerbates atherosclerosis through activation of brown fat-mediated lipolysis, Proc. Natl. Acad. Sci. USA 116 (22) (2019) 10937–10942.
[9] M. Westerterp, C.C. van der Hoogt, W. de Haan, E.H. Offerman, G.M. Dallinga-Thie, J.W. Jukema, L.M. Havekes, P.C. Rensen, Cholesteryl ester transfer protein decreases high-density lipoprotein and severely aggravates atherosclerosis in APOE*3-Leiden mice, Arterioscler. Thromb. Vasc. Biol. 26 (11) (2006) 2552–2559.
[10] W. de Haan, J. de Vries-van der Weij, J.W. van der Hoorn, T. Gautier, C.C. van der Hoogt, M. Westerterp, J.A. Romijn, J.W. Jukema, L.M. Havekes, H.M. Princen, P. C. Rensen, Torcetrapib does not reduce atherosclerosis beyond atorvastatin and induces more proinflammatory lesions than atorvastatin, Circulation 117 (19) (2008) 2515–2522.
[11] E. Zhou, Z. Li, H. Nakashima, A. Choukoud, S. Kooijman, J.F.P. Berbée, P.C. N. Rensen, Y. Wang, Beneficial effects of brown fat activation on top of PCSK9 inhibition with alirocumab on dyslipidemia and atherosclerosis development in APOE*3-Leiden.CETP mice, Pharm. Res 167 (2021), 105524.
[12] R. van Eenige, P.S. Verhave, P.J. Koemans, I. Tiebosch, P.C.N. Rensen, S. Kooijman, RandoMice, a novel, user-friendly randomization tool in animal research, PLoS One 15 (8) (2020), e0237096.
[13] Z. Ying, M.R. Boon, T. Coskun, S. Kooijman, P.C.N. Rensen, A simplified procedure to trace triglyceride-rich lipoprotein metabolism in vivo, Physiol. Rep. 9 (8) (2021), e14820.
[14] M.C. Jong, P.C. Rensen, V.E. Dahlmans, H. van der Boom, T.J. van Berkel, L. M. Havekes, Apolipoprotein C-III deficiency accelerates triglyceride hydrolysis by lipoprotein lipase in wild-type and apoE knockout mice, J. Lipid Res 42 (10) (2001) 1578–1585.
[15] E.G. Bligh, W.J. Dyer, A rapid method of total lipid extraction and purification, Can. J. Biochem Physiol. 37 (8) (1959) 911–917.
[16] M.C. Wong, J.A. van Diepen, L. Hu, B. Guigas, H.C. de Boer, G.H. van Puijvelde, J. Kuiper, A.J. van Zonneveld, S.E. Shoelson, P.J. Voshol, J.A. Romijn, L. M. Havekes, J.T. Tamsma, P.C. Rensen, P.S. Hiemstra, J.F. Berbée, Hepatocyte-specific IKKβ expression aggravates atherosclerosis development in APOE*3-Leiden mice, Atherosclerosis 220 (2) (2012) 362–368.
[17] S.R. Wang, G. Renaud, J. Infante, D. Catala, R. Infante, Isolation of rat hepatocytes with EDTA and their metabolic functions in primary culture, Vitr. Cell Dev. Biol. 21 (9) (1985) 526–530.
[18] J.A. van Diepen, M.C. Wong, B. Guigas, J. Bos, R. Stienstra, L. Hodson, S. E. Shoelson, J.F. Berbée, P.C. Rensen, J.A. Romijn, L.M. Havekes, P.J. Voshol, Hepatocyte-specific IKK-β activation enhances VLDL-triglyceride production in APOE*3-Leiden mice, J. Lipid Res 52 (5) (2011) 942–950.
[19] M.D. Jensen, V. Chandramouli, W.C. Schumann, K. Ekberg, S.F. Previs, S. Gupta, B. R. Landau, Sources of blood glycerol during fasting, Am. J. Physiol. Endocrinol. Metab. 281 (5) (2001) E998–E1004.
[20] R.S. Gordon, Jr, Unesterified fatty acid in human blood plasma. II. The transport function of unesterified fatty acid, J. Clin. Invest 36 (6 Part 1) (1957) 81085.

[21] M. Alves-Bezerra, D.E. Cohen, Triglyceride Metabolism in the Liver, Compr. Physiol. 8 (1) (2017) 1–8.
[22] M. Heine, A.W. Fischer, C. Schlein, C. Jung, L.G. Straub, K. Gottschling, N. Mangels, Y. Yuan, S.K. Nilsson, G. Liebscher, O. Chen, R. Schreiber, R. Zechner, L. Scheja, J. Heeren, Lipolysis triggers a systemic insulin response essential for efficient energy replenishment of activated brown adipose tissue in mice, Cell Metab. 28 (4) (2018) 644–655, e4.
[23] D.P. Blondin, S. Nielsen, E.N. Kuipers, M.C. Severinsen, V.H. Jensen, S. Miard, N. Z. Jespersen, S. Kooijman, M.R. Boon, M. Fortin, S. Phoenix, F. Frisch, B. Guérin, E. Turcotte, É., F. Haman, D. Richard, F. Picard, P.C.N. Rensen, C. Scheele, A. C. Carpentier, Human brown adipocyte thermogenesis is driven by β2-AR stimulation, Cell Metab. 32 (2) (2020) 287–300, e7.
[24] L. Hao, S. Scott, M. Abbasi, Y. Zu, M.S.H. Khan, Y. Yang, D. Wu, L. Zhao, S. Wang, Beneficial metabolic effects of mirabegron in vitro and in high-fat diet-induced obese mice, J. Pharm. Exp. Ther. 369 (3) (2019) 419–427.
[25] A.M. Cypess, L.S. Weiner, C. Roberts-Toler, E. Franquet Elia, S.H. Kessler, P. A. Kahn, J. English, K. Chatman, S.A. Trauger, A. Doria, G.M. Kolodny, Activation of human brown adipose tissue by a beta3-adrenergic receptor agonist, Cell Metab. 21 (1) (2015) 33–38.
[26] B.S. Finlin, H. Memetimin, A.L. Confides, I. Kasza, B. Zhu, H.J. Vekaria, B. Harfmann, K.A. Jones, Z.R. Johnson, P.M. Westgate, C.M. Alexander, P. G. Sullivan, E.E. Dupont-Versteegden, P.A. Kern, Human adipose beiging in response to cold and mirabegron, JCI Insight 3 (15) (2018).
[27] A.E. O'Mara, J.W. Johnson, J.D. Linderman, R.J. Brychta, S. McGehee, L. A. Fletcher, Y.A. Fink, D. Kapuria, T.M. Cassimatis, N. Kelsey, C. Cero, Z. Abdul-Sater, F. Piccinini, A.S. Baskin, B.P. Leitner, H. Cai, C.M. Millo, W. Dieckmann, M. Walter, N.B. Javitt, Y. Rotman, P.J. Walter, M. Ader, R.N. Bergman, P. Herscovitch, K.Y. Chen, A.M. Cypess, Chronic mirabegron treatment increases human brown fat, HDL cholesterol, and insulin sensitivity, J. Clin. Invest 130 (5) (2020) 2209–2219.
[28] K.J. Nahon, L.G.M. Janssen, A.S.D. Sardjoe Mishre, M.P. Bilsen, J.A. van der Eijk, K. Botani, L.A. Overduin, J.R. Ruiz, J. Burakiewicz, O. Dzyubachyk, A.G. Webb, H. E. Kan, J.F.P. Berbée, J.B. van Klinken, K.W. van Dijk, M. van Weeghel, F.M. Vaz, T. Coskun, I.M. Jazet, S. Kooijman, B. Martinez-Tellez, M.R. Boon, P.C.N. Rensen, The effect of mirabegron on energy expenditure and brown adipose tissue in healthy lean South Asian and Europid men, Diabetes Obes. Metab. 22 (11) (2020) 2032–2044.
[29] C. Peres Valgas da Silva, F. Calmasini, E.C. Alexandre, H.F. Raposo, M.A. Delbin, F. Z. Monica, A. Zanesco, The effects of mirabegron on obesity-induced inflammation and insulin resistance are associated with brown adipose tissue activation but not beiging in the subcutaneous white adipose tissue, Clin. Exp. Pharm. Physiol. 48 (11) (2021) 1477–1487.
[30] C. Liu, M. Schönke, E. Zhou, Z. Li, S. Kooijman, M.R. Boon, M. Larsson, K. Wallenius, N. Dekker, L. Barlind, X.R. Peng, Y. Wang, P.C.N. Rensen, Pharmacological treatment with FGF21 strongly improves plasma cholesterol metabolism to reduce atherosclerosis, Cardiovasc Res (2021).
[31] A. Bartelt, C. John, N. Schaltenberg, J.F.P. Berbee, A. Worthmann, M.L. Cherradi, C. Schlein, J. Piepenburg, M.R. Boon, F. Rinninger, M. Heine, K. Toedter, A. Niemeier, S.K. Nilsson, M. Fischer, S.L. Wijers, W. van Marken Lichtenbelt, L. Scheja, P.C.N. Rensen, J. Heeren, Thermogenic adipocytes promote HDL turnover and reverse cholesterol transport, Nat. Commun. 8 (2017) 15010.
[32] E. Zhou, Z. Li, H. Nakashima, C. Liu, Z. Ying, A.C. Foks, J.F.P. Berbée, K.W. van Dijk, P.C.N. Rensen, Y. Wang, Hepatic scavenger receptor class b type 1 knockdown reduces atherosclerosis and enhances the antiatherosclerotic effect of brown fat activation in APOE*3-Leiden.CETP Mice, Arterioscler. Thromb. Vasc. Biol. 41 (4) (2021) 1474–1486.
[33] R.A. Takx, A. Ishai, Q.A. Truong, M.H. MacNabb, M. Scherrer-Crosbie, A. Tawakol, Supraclavicular brown adipose tissue 18F-FDG uptake and cardiovascular disease, J. Nucl. Med 57 (8) (2016) 1221–1225.
[34] T. Becher, S. Palanisamy, D.J. Kramer, M. Eljalby, S.J. Marx, A.G. Wibmer, S. D. Butler, C.S. Jiang, R. Vaughan, H. Schöder, A. Mark, P. Cohen, Brown adipose tissue is associated with cardiometabolic health, Nat. Med 27 (1) (2021) 58–65.
[35] J. Raiko, J. Orava, N. Savisto, K.A. Virtanen, High brown fat activity correlates with cardiovascular risk factor levels cross-sectionally and subclinical atherosclerosis at 5-year follow-up, Arterioscler. Thromb. Vasc. Biol. 40 (5) (2020) 1289–1295.
[36] T.M. Larsen, S. Toubro, M.A. van Baak, K.M. Gottesdiener, P. Larson, W.H. Saris, A. Astrup, Effect of a 28-d treatment with L-796568, a novel beta(3)-adrenergic receptor agonist, on energy expenditure and body composition in obese men, Am. J. Clin. Nutr. 76 (4) (2002) 780–788.
[37] L.M. Redman, L. de Jonge, X. Fang, B. Gamlin, D. Recker, F.L. Greenway, S. R. Smith, E. Ravussin, Lack of an effect of a novel beta3-adrenoceptor agonist, TAK-677, on energy metabolism in obese individuals: a double-blind, placebo-controlled randomized study, J. Clin. Endocrinol. Metab. 92 (2) (2007) 527–531.